Journal of Electroceramics, 9, 5–16, 2002

Grain-Boundary Effect on the Curie-Weiss Law of Ferroelectric Ceramics and Polycrystalline Thin Films: Calculation by the Method of Effective Medium

A.YU. EMELYANOV,[1] N.A. PERTSEV,[1,2] S. HOFFMANN-EIFERT,[2] U. BÖTTGER[3] & R. WASER[2,3]

[1]*A. F. Ioffe Physico-Technical Institute, Russian Academy of Sciences, 194021 St. Petersburg, Russia*

[2]*Institute für Festkörperforschung, Forschungszentrum Jülich, D-52425 Jülich, Germany*

[3]*Institut für Werkstoffe der Elektrotechnik, RWTH Aachen University of Technology, D-52056 Aachen, Germany*

Submitted June 27, 2002; Revised June 27, 2002; Accepted September 18, 2002

Abstract. The influence of grain boundaries on the dielectric properties of ferroelectric ceramics and polycrystalline thin films is described theoretically by the method of effective medium. Grain boundaries are modeled by low-permittivity ("dead") layers, which do not exhibit ferroelectric instability. The effective permittivity of a polycrystalline material is calculated in the paraelectric regime above the transition temperature. The calculations are based on the solution of electrostatic problem for a spherical dielectric inclusion separated from the surrounding dissimilar matrix by a low-permittivity interface layer. For isotropic bulk ceramics, an analytic expression is derived for the effective permittivity as a function of the grain size, dead-layer thickness, and its permittivity. Temperature dependence of the aggregate dielectric response is calculated for $BaTiO_3$ (BT) ceramics of different grain sizes and found to be in good agreement with measurements. It is shown that grain boundaries not only renormalize the Curie-Weiss temperature and constant, but may also cause deviations from the Curie-Weiss law. For BT polycrystalline thin films grown on dissimilar substrates, numerical calculations of the effective dielectric constants are performed, taking into account both the grain-boundary and substrate effects on the film anisotropic dielectric response. Theoretical predictions are compared with the grain size dependence of the permittivity of BT films grown on Pt-coated Si.

Keywords: ferroelectric ceramics, polycrystalline thin films, grain boundaries, dielectric properties, effective-medium approximation

1. Introduction

Size effects on the microstructure and physical properties of ferroelectric crystals, thin films, and ceramics are presently attracting great interest in view of numerous current and potential applications of ferroelectric materials in the modern microelectronics [1]. Various possible causes for the existence of the crystal-size effects in ferroelectrics were discussed in the literature (for an overview, see, e.g., Refs. [1–3]).

For ferroelectric ceramics, the dependence of dielectric response on the grain size was first observed already in 1954 [4]. Kinoshita and Yamaji [5] studied the dielectric properties of $BaTiO_3$ (BT) ceramics with the grain size down to 1.1 μm, whereas Arlt et al. [6] extended the studied range of grain sizes to 280 nm. The increase of the dielectric constant in fine-grained ferroelectric ceramics below the Curie temperature has been attributed either to an increase in residual internal stress in submicron grains [7] or to the enhanced domain-wall contribution [6]. Both these explanations, however, cannot be used to describe a relative decrease of the ceramic permittivity ε above the Curie temperature, which was also observed in submicron BT ceramics [8, 9]. A detailed study of BT ceramics having grain sizes between 2000 nm and 70 nm, which was performed by Frey et al. [8, 9], showed that the dependence of ε on temperature T still obeys the Curie-Weiss

law $\varepsilon \sim (T - \theta^*)^{-1}$ in the paraelectric regime. The apparent Curie-Weiss temperature θ^*, however, depends on the grain size g and differs considerably from the single-crystal value of $\theta = 110^\circ$C at $g \leq 300$ nm.

The observed dielectric behavior of BT polycrystals has been attributed to the presence of a low-permittivity phase at the boundaries between adjacent grains [8, 9]. The aggregate macroscopic dielectric response of a polycrystalline material was calculated using a simple relationship derived earlier by Payne and Cross [10]. These authors successfully described the measured dielectric properties for a composite comprised of grains with a high permittivity separated by a thin continuous low-permittivity boundary phase in terms of series dielectric mixing. They used the brick-wall model of polycrystalline microstructure to derive an approximate expression for the macroscopic dielectric constant ε_m of an isotropic composite. According to this expression, ε_m depends on the permittivities ε_f and ε_d of two dissimilar phases present in a heterogeneous material, their volume fractions, and on a geometric factor f related to the microstructure geometry. (A value of $f = 1/3$ represents the condition of $\varepsilon_f \gg \varepsilon_d$ for cube-shaped grains.) Frey et al. [8, 9] have shown that the grain-size dependence of the dielectric response ε_m observed in BT ceramics can be reproduced with a good accuracy by taking the grain-boundary relative permittivity of $\varepsilon_d = 130$ and thickness of $d = 0.8$ nm and assuming $f = 0.8$. Though the series dielectric-mixing rule provides a useful approximation for the grain-boundary effect on the permittivity of bulk ceramics, this effect evidently calls for the further rigorous theoretical analysis.

Moreover, the grain-size effect on the dielectric properties was also observed in polycrystalline thin films [11]. Hoffmann and Waser have found that the permittivity of BT films grown on platinum coated silicon substrates reduces with decreasing grain size [11]. Remarkably, the out-of-plane dielectric response ε_c appears to be well below that of coarse-grained BT ceramics even in a columnar-structured film, where the grain-boundary effect must be negligible. Nevertheless, the temperature dependence of ε_c still follows the Curie-Weiss law at high temperatures, but with different parameters. This renormalization of the Curie-Weiss law in a columnar-structured film was successfully explained by the mechanical film/substrate interaction [12]. Additional reduction of the permittivity in fine-grained films may be attributed to the presence of grain boundaries orthogonal to the measuring electric field.

Thus, the influence of grain boundaries on the dielectric properties of polycrystalline ferroelectrics requires further theoretical analysis. In this paper, we study the problem in the effective medium approximation [13]. To calculate the macroscopic dielectric response of a polycrystalline material, we employ the model of a representative spherical grain surrounded by a homogeneous matrix. The grain is assumed to consist of a ferroelectric core and an interface layer with a temperature-independent permittivity, which models the grain boundary. By solving a relevant electrostatic problem and using the self-consistent scheme, it becomes possible to compute the effective dielectric constants of bulk ceramics and polycrystalline thin films, taking into account both the grain-boundary and substrate effects in the latter case.

2. Coated Isotropic Inclusion in a Uniform Electric Field

Consider a spherical dielectric inclusion coated by a layer with another permittivity and embedded into an infinite homogeneous medium (see Fig. 1). Dielectric properties of the inclusion, interface layer, and matrix are assumed to be isotropic in this section; they will be defined by relative permittivities ε_f, ε_d, and ε_m, respectively. Suppose now that the introduced material system is subjected to a uniform electric field $\mathbf{E}_0$ at

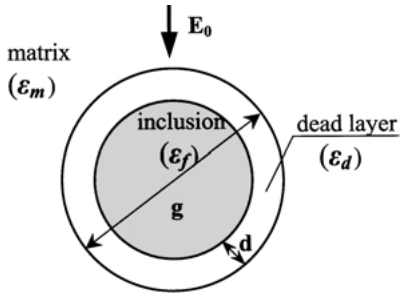

Fig. 1. Spherical dielectric inclusion coated by a thin interface layer and embedded into a dissimilar matrix. The thickness of interface layer is d and the radius of inclusion is $R = (g - 2d)/2$. Dielectric properties of the inclusion, interface layer, and matrix are assumed to be isotropic; their permittivities are denoted by ε_f, ε_d, and ε_m, respectively. $\mathbf{E}_0$ is a uniform external electric field in the matrix at large distances from the inclusion.

large distances from the coated sphere. The perturbation of this field by the dielectric inhomogeneity can be calculated by analogy with the classical solution, which was obtained for a dielectric ellipsoid in an external field [14]. For the local electric fields $\mathbf{E}^{(f)}$, $\mathbf{E}^{(d)}$, and $\mathbf{E}^{(m)}$ in the spherical inclusion, interface layer, and matrix, we derived the following analytic expressions:

$$\mathbf{E}^{(f)} = 9\frac{\varepsilon_m}{\varepsilon_f K}\mathbf{E}_0, \tag{1}$$

$$\mathbf{E}^{(d)} = 3\frac{\varepsilon_m}{\varepsilon_d K}\left\{\left(1+2\frac{\varepsilon_d}{\varepsilon_f}\right)\mathbf{E}_0 + \left(1-\frac{\varepsilon_d}{\varepsilon_f}\right)\left(\frac{R}{r}\right)^3 \times\left[3(\mathbf{E}_0\cdot\mathbf{r})\frac{\mathbf{r}}{r^2}-\mathbf{E}_0\right]\right\}, \tag{2}$$

$$\mathbf{E}^{(m)} = \mathbf{E}_0 + \left\{1+3\frac{\varepsilon_m}{\varepsilon_d K}\left[\left(1-\frac{\varepsilon_d}{\varepsilon_f}\right)\left(\frac{R}{R+d}\right)^3 - 1 - 2\frac{\varepsilon_d}{\varepsilon_f}\right]\right\}\left(\frac{R+d}{r}\right)^3\left[3(\mathbf{E}_0\cdot\mathbf{r})\frac{\mathbf{r}}{r^2}-\mathbf{E}_0\right], \tag{3}$$

where $\mathbf{r}$ is the radius-vector with respect to the sphere center, R is the inclusion radius, d is the thickness of interface layer, and the dimensionless parameter K equals

$$K = \left(1+2\frac{\varepsilon_m}{\varepsilon_d}\right)\left(1+2\frac{\varepsilon_d}{\varepsilon_f}\right) + 2\left(\frac{R}{R+d}\right)^3 \times\left(1-\frac{\varepsilon_m}{\varepsilon_d}\right)\left(1-\frac{\varepsilon_d}{\varepsilon_f}\right). \tag{4}$$

The fields (1)–(3) represent a *unique* solution of the considered electrostatic problem, which satisfies the boundary conditions on the interfaces between dissimilar materials, i.e. the continuity of the tangential component of electric field $\mathbf{E}$ and the normal component of the electric displacement $\mathbf{D} = \varepsilon_0\,\varepsilon\,\mathbf{E}$ (ε_0 is the permittivity of the vacuum). Remarkably, the electric field $\mathbf{E}^{(f)}$ inside the isotropic dielectric inclusion remains *uniform*. The fields $\mathbf{E}^{(d)}$ and $\mathbf{E}^{(m)}$ in the interface layer and matrix are *inhomogeneous* and contain a component proportional to $3(\mathbf{E}_0\cdot\mathbf{r})\mathbf{r}/r^5 - \mathbf{E}_0/r^3$, which varies in space as a field of an *electrical point dipole* [15] situated at the inclusion center.[1]

Polarizations $\mathbf{P}^{(f)}$, $\mathbf{P}^{(d)}$, and $\mathbf{P}^{(m)}$, which are induced in the inclusion, interface layer, and matrix by an external field $\mathbf{E}_0$, can be easily found with the aid of Eqs. (1)–(3) as $\mathbf{P}^{(i)}(\mathbf{r}) = \varepsilon_0(\varepsilon_i - 1)\mathbf{E}^{(i)}(\mathbf{r})$ ($i = f, d, m$).

The average polarization $\langle\mathbf{P}_g\rangle$ of the whole inclusion can be calculated by integrating the local polarization $\mathbf{P}(\mathbf{r})$ over the volume of the coated sphere of radius $R+d$. From the symmetry of isotropic inclusion/matrix system it immediately follows that the average electric field inside the coated sphere is parallel to the external field $\mathbf{E}_0$. Therefore, the vector $\langle\mathbf{P}_g\rangle$ is parallel to the external field $\mathbf{E}_0$ too. The integration of Eqs. (1)–(2) leads to an analytic expression for the average polarization $\langle\mathbf{P}_g\rangle$ in the coated sphere, which has the form

$$\langle\mathbf{P}_g\rangle = 3\varepsilon_0\frac{\varepsilon_m}{K}\left(\frac{R}{R+d}\right)^3\left(1-\frac{1}{\varepsilon_f}\right) + \left(1-\frac{1}{\varepsilon_d}\right) \times\left(1+2\frac{\varepsilon_d}{\varepsilon_f}\right)\left[\left(\frac{R+d}{R}\right)^3 - 1\right]\mathbf{E}_0, \tag{5}$$

where the parameter K is given by Eq. (4). Substituting Eq. (5) into the relation $\langle\varepsilon_g\rangle = 1 + \langle\mathbf{P}_g\rangle/(\varepsilon_0\mathbf{E}_0)$, we can also find the average dielectric response $\langle\varepsilon_g\rangle$ of the coated inclusion.

3. Grain-size Effect on the Curie-Weiss Law in Bulk Ceramics

3.1. Calculation of Ceramic Permittivity by the Method of Effective Medium

In the effective medium approximation, the aggregate material constants of a polycrystal are set equal to the average constants of individual grains. To calculate the unknown effective permittivity of an isotropic bulk ceramic, therefore, we must assume that the average dielectric response $\langle\varepsilon_g\rangle$ of the grain is equal to the matrix dielectric constant ε_m. Setting $\langle\mathbf{P}_g\rangle/(\varepsilon_0\mathbf{E}_0) = \varepsilon_m - 1$ in Eq. (5), we obtain the following *quadratic* equation for the ceramic permittivity ε_m

$$\left[\left(1+2\frac{\varepsilon_m}{\varepsilon_d}\right)\left(1+2\frac{\varepsilon_d}{\varepsilon_f}\right) + 2\left(\frac{g-2d}{g}\right)^3 \times\left(1-\frac{\varepsilon_m}{\varepsilon_d}\right)\left(1-\frac{\varepsilon_d}{\varepsilon_f}\right)\right]\left(1-\frac{1}{\varepsilon_m}\right) = 3\left(\frac{g-2d}{g}\right)^3\left\{3\left(1-\frac{1}{\varepsilon_f}\right) + \left(1-\frac{1}{\varepsilon_d}\right) \times\left(1+2\frac{\varepsilon_d}{\varepsilon_f}\right)\left[\left(\frac{g}{g-2d}\right)^3 - 1\right]\right\}, \tag{6}$$

where $g = 2(R + d)$ is the grain size. Equation (6) is valid for any magnitudes of the dielectric constants ε_m, ε_f, and ε_d. Fortunately, in the case of ferroelectric ceramics it may be reduced to a *linear* equation with a high accuracy because the dielectric constant ε_m is much larger than unity. The solution of this equation reads

$$\varepsilon_m \cong \frac{3\varepsilon_d(\varepsilon_f + 2\varepsilon_d)}{\varepsilon_f + 2\varepsilon_d - (\varepsilon_f - \varepsilon_d)\left(\frac{g-2d}{g}\right)^3} - 2\varepsilon_d. \quad (7)$$

Equation (7) may be used to predict the temperature dependence of the ceramic permittivity in the paraelectric regime. Since the grain core possesses a ferroelectric instability, the dependence of its permittivity ε_f on temperature T should obey the Curie-Weiss law $\varepsilon \cong C/(T - \theta)$, where θ and C are the Curie-Weiss temperature and constant of a single crystal. The dielectric constant ε_d of an interfacial low-permittivity layer, which models the grain boundary, may be taken as a constant parameter because its temperature dependence is negligible relative to $\varepsilon_f(T)$. Substituting $\varepsilon_f = C/(T - \theta)$ into Eq. (7), after some mathematical manipulation we obtain

$$\varepsilon_m \cong \frac{C^* + B(T - \theta)}{T - \theta^*}, \quad (8)$$

$$\theta^* = \theta - \frac{C}{\varepsilon_d}\frac{[g^3 - (g - 2d)^3]}{[2g^3 + (g - 2d)^3]}, \quad (9)$$

$$C^* = C\frac{[g^3 + 2(g - 2d)^3]}{[2g^3 + (g - 2d)^3]}, \quad (10)$$

$$B = \varepsilon_d\frac{2[g^3 - (g - 2d)^3]}{[2g^3 + (g - 2d)^3]}. \quad (11)$$

It can be seen that, in the presence of "dead" grain-boundary layers, the ceramic permittivity $\varepsilon_m(T)$ follows a *modified* Curie-Weiss law, where the numerator is also temperature-dependent. However, in a temperature range $|T - \theta| \ll |C^*/B|$ the second term in the numerator on the right-hand side of Eq. (8) can be neglected. Accordingly, the standard Curie-Weiss behavior is restored in a certain temperature range near θ.

Figure 2 shows representative temperature dependences of the inverse of the permittivity, $1/\varepsilon_m$, computed for BT ceramics with the aid of the general relation (6). It can be seen that, when the volume fraction of the grain-boundary phase and its permittivity are relatively small ($d/g < 0.1$ and $\varepsilon_d \leq 100$), the grain boundaries do not cause significant deviations

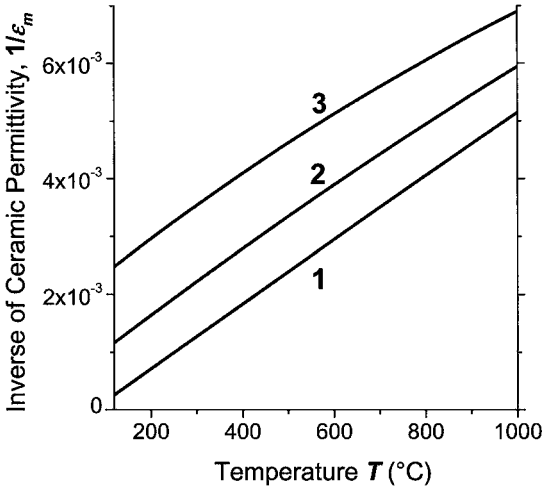

Fig. 2. Temperature dependences of the inverse of the permittivity, $1/\varepsilon_m$, calculated for bulk $BaTiO_3$ ceramics having different volume fractions of the low-permittivity grain-boundary phase: $d/g = 0.01$ (curve 1), $d/g = 0.05$ (curve 2), $d/g = 0.1$ (curve 3). The permittivity of grain cores varies with temperature T as $\varepsilon_f = 1.8 \times 10^5/(T - 110°\text{C})$. The dielectric constant of grain-boundary regions is assumed to be $\varepsilon_d = 100$.

of $1/\varepsilon_m(T)$ from the linear dependence even at large $|T - \theta|$. The analysis of Eqs. (8)–(11) demonstrates that strong deviations from the Curie-Weiss law may appear only in polycrystals with the grain-boundary phase having a high (but temperature-independent) permittivity of $\varepsilon_d \sim 1000$.

In properly processed ceramics, the grain boundaries are expected to be only a few lattice spacings thick [9]. For such materials, the ratio d/g should be less than 0.02 even in fine-grained polycrystals with $g \sim 100$ nm. Based on the measured dielectric properties of nonferroelectric titanates [16], the permittivity $\varepsilon_d \sim 100$ may be attributed to the (structurally disordered) grain-boundary phase in BT and similar perovskite ceramics. With the above values of d/g and ε_d, Eqs. (8)–(11) predict that grain boundaries mainly renormalize the Curie-Weiss temperature and constant (relative to their single-crystal values θ and C) without visible deviations from the Curie-Weiss law in perovskite ferroelectric ceramics. This conclusion agrees with the experimental data on BT ceramics and the earlier theoretical prediction, which follows from the brick-wall model [8, 9].

The influence of grain boundaries on the effective Curie-Weiss parameters θ^* and C^* is described by Eqs. (9) and (10) and has the following features.

(i) The renormalized Curie-Weiss temperature θ^* is always *lower* than θ.
(ii) The value of θ^* decreases monotonically with decreasing permittivity ε_d and increasing thickness d of the grain boundary (since $\partial\theta^*/\partial\varepsilon_d$ is positive, whereas $\partial\theta^*/\partial d$ is negative).
(iii) The Curie-Weiss constant C^* is independent of the grain-boundary permittivity ε_d. The value of C^* decreases monotonically with increasing grain-boundary thickness $d(\partial C^*/\partial d < 0)$.
(iv) In the typical case of $d/g \ll 1$, the deviations of renormalized parameters from the single-crystal values are *directly proportional* to the relative thickness d/g of the grain boundaries. In the first approximation, the parameters θ^* and C^* can be calculated from the relations

$$\theta^* \approx \theta - 2\frac{C}{\varepsilon_d}\frac{d}{g}, \quad C^* \approx C\left(1 - 2\frac{d}{g}\right). \qquad (12)$$

3.2. *Comparison between Theory and Experiment*

For the quantitative theoretical prediction of the ceramic permittivity $\varepsilon_m(T)$, the mean grain-boundary thickness d and its permittivity ε_d must be known to a good degree of precision. In the absence of such data (being difficult to obtain experimentally), ε_d and d may be regarded as adjustable parameters, which can be extracted from the fitting of experimental dependences $\varepsilon(T)$ measured for a set of ceramics with different grain size g.

If the dielectric response of a polycrystalline material demonstrates the Curie-Weiss behavior in the paraelectric regime, the effective characteristics d and ε_d of the grain boundaries existing in this material can be determined via the following two-step procedure. First, from the observed grain-size dependence of the Curie-Weiss constant C^* one can evaluate the mean thickness d of grain boundaries with the aid of Eq. (10). Second, the permittivity ε_d of grain boundaries can be found by fitting the dependence $\theta^*(g)$ by Eq. (9) with the obtained value of d.

Now we can proceed to the analysis of the Curie-Weiss behavior demonstrated by fine-grained BT ceramics [8, 9]. Figure 3 shows the grain-size dependence of the Curie-Weiss parameters θ^* and C^*, which were extracted from the experimental data on the ceramic permittivities $\varepsilon(T, g)$ given in Ref. 8 and 9. It can be seen that the Curie-Weiss temperature θ^* decreases

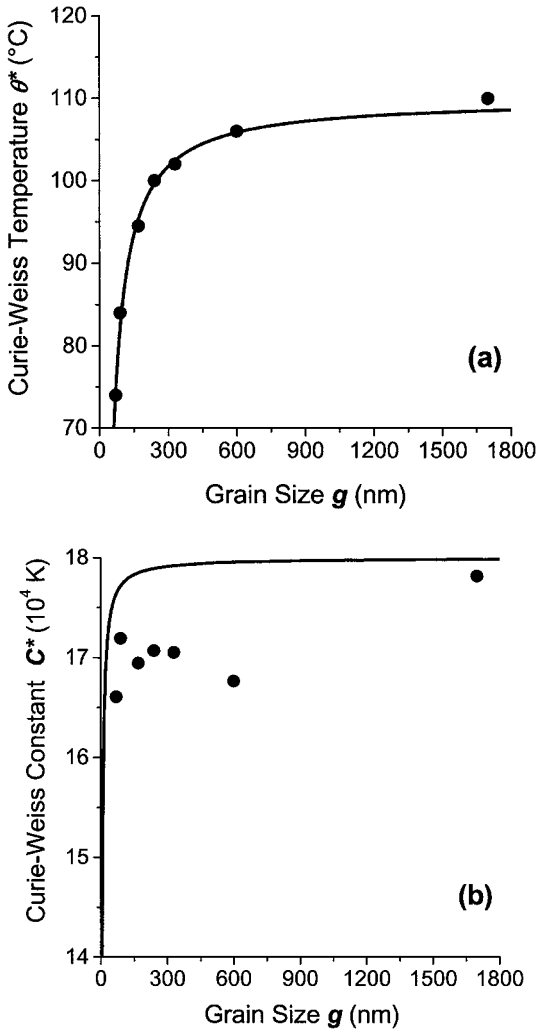

Fig. 3. Grain-size dependence of the Curie-Weiss temperature (a) and constant (b) in bulk $BaTiO_3$ ceramics. The experimental data points were extracted from the measured temperature dependences of the ceramic permittivities $\varepsilon(T, g)$, which were reported in Refs. [8, 9] for the temperature range between 150°C and 200°C, where there are no substantial deviations from the Curie-Weiss law. The theoretical curves $\theta^*(g)$ and $C^*(g)$ were computed using Eqs. (9) and (10), respectively. The involved material parameters were taken to be $\theta = 110$°C, $C = 1.8 \times 10^5$ K, $\varepsilon_d = 100$, and $d = 0.7$ nm.

gradually with decreasing grain size. The dependence $C^*(g)$, however, cannot be determined unambiguously because the scatter in the experimental values of C^* is too large.

In this situation, the simultaneous separate determination of two grain-boundary characteristics, d and ε_d, cannot give reliable results. Therefore, we first used Eq. (9) to fit the dependence $\theta^*(g)$. The single-crystal

values of the Curie-Weiss parameters for BT were taken to be $\theta = 110^{\circ}$C and $C = 1.8 \times 10^5$ K [17]. The calculation showed that the observed grain-size dependence of the Curie-Weiss temperature θ^* can be fitted almost perfectly by taking the ratio $d/\varepsilon_d = 0.007$ nm [see Fig. 3(a)]. [According to Eq. (12), $\theta^*(g)$ mainly depends on the ratio d/ε_d, but not on individual values of d and ε_d.] Using this value of d/ε_d we obtain the estimate $d \approx 0.7$ nm for the thickness of grain boundaries in BT since their permittivity, as mentioned above, is expected to be about 100. The theoretical dependence $C^*(g)$, calculated at $d = 0.7$ nm, is in reasonable agreement with the experimental data [see Fig. 3(b)].

The above estimate of the grain-boundary thickness in BT ceramics is close to that obtained by Frey et al. on the basis of the brick-wall model ($d = 0.8$ nm) [8, 9]. However, it should be noted that the parameter d involved in our calculations represents an *apparent thickness* of grain boundaries rather than their actual transverse size. Indeed, the effective thickness d characterizes only the influence of grain boundaries on the distribution of electric field so that d may differ from the average thickness of structurally disordered layers between crystallites. Moreover, in the framework of the effective medium approach, the coated spherical inclusion serves also as a building block, which is used to construct the dielectric matrix. Accordingly, the size d of the interfacial low-permittivity layer is expected to be closer to the *half* of the actual grain-boundary thickness. Therefore, we believe that in BT ceramics the latter is from three to four lattice spacings.

4. Renormalization of the Curie-Weiss Law in $BaTiO_3$ Polycrystalline Thin Films

4.1. Computation of the Film Permittivity in the Effective Medium Approximation

In this section, we use the effective medium approximation to calculate the dielectric responses of polycrystalline ferroelectric films grown on dissimilar substrates. This problem is complicated by the dielectric anisotropy, which is inherent in such films even in the paraelectric regime. The anisotropy is due to the two-dimensional straining of the film, induced by a much thicker substrate during the deposition process and/or the subsequent cooling [18].

In perovskite films grown on (001)-oriented cubic or tetragonal substrates, the macroscopic dielectric properties are isotropic in the film plane [19]. Accordingly, they can be defined by the out-of-plane (ε_c^m) and in-plane (ε_a^m) permittivities. This uniaxial anisotropy should be now attributed to the dielectric matrix in our model shown in Fig. 1. The dielectric properties of individual crystallites depend on the orientation of their crystallographic axes with respect to the substrate normal (c axis). For the paraelectric state, this dependence is caused solely by the electrostrictive effect. In crystallites having one of the four-fold axes parallel to the substrate normal, the dielectric response also possesses the uniaxial anisotropy. The out-of-plane and in-plane permittivities of such crystallites are defined by the relations [18]

$$\varepsilon_c^f = 1 + \frac{1}{2\varepsilon_0\left[\alpha_1 - S_m 2Q_{12}/(s_{11} + s_{12})\right]}, \tag{13}$$

$$\varepsilon_a^f = 1 + \frac{1}{2\varepsilon_0\left[\alpha_1 - S_m(Q_{11} + Q_{12})/(s_{11} + s_{12})\right]}, \tag{14}$$

where $\alpha_1 = (T - \theta)/(2\varepsilon_0 C)$ is the dielectric stiffness of the ferroelectric, Q_{ij} and s_{ij} are the electrostrictive constants and elastic compliances of the paraelectric phase, and S_m is the misfit strain in the film/substrate system, which is discussed in detail below. To simplify the calculations, we assume in this work that all crystallites in the film have the above spatial orientation of the crystallographic axes. In this approximation of a fully textured polycrystalline film, the inclusion in our model material system may be given a uniaxial dielectric anisotropy with the symmetry axis parallel to that of the matrix. Evidently, the dielectric response of the interface "dead" layer still may be taken to be isotropic.

To calculate the macroscopic dielectric constants ε_c^m and ε_a^m of a polycrystalline film in the effective medium approximation, it is necessary to find first the local electric fields $\mathbf{E}^{(f)}(\mathbf{r})$ and $\mathbf{E}^{(d)}(\mathbf{r})$, which are induced in the inclusion and interface layer by a uniform field $\mathbf{E}_0$ applied to the matrix. Our analysis showed that, in the presence of both the dielectric anisotropy and a dissimilar interface layer, an analytic solution of this electrostatic problem seems to be impossible. Hence we carried out numerical calculations of the electric-field distribution in our model material system using the procedure described in the Appendix. Figure 4 shows representative maps of equipotential lines inside and outside the coated inclusion, which were computed at different values of the factor $\varepsilon_c^f/\varepsilon_a^f$ that characterizes the inclusion anisotropy. It can be seen that the

field distribution inside the inclusion is sensitive to the degree of its dielectric anisotropy. According to our computations, the matrix anisotropy $\varepsilon_c^m/\varepsilon_a^m$, dead layer thickness d, and its permittivity ε_d also affect the distribution of electric field.

Using the calculated fields $\mathbf{E}^{(f)}(\mathbf{r})$ and $\mathbf{E}^{(d)}(\mathbf{r})$, it is possible to evaluate the average polarization $\langle P_g \rangle$, which is induced in the coated inclusion by an external electric field $\mathbf{E}_0$. Hence one can easily determine the effective dielectric responses $\langle \varepsilon_c^g \rangle$ and $\langle \varepsilon_a^g \rangle$ of the coated inclusion, measured along the symmetry axis c of the material system and orthogonal to this axis. A convenient way to calculate these responses is to consider separately the two basic orientations of the field $\mathbf{E}_0$, i.e., those parallel and perpendicular to the c axis. Then the magnitudes of $\langle \varepsilon_c^g \rangle$ and $\langle \varepsilon_a^g \rangle$ will be defined simply by the ratio of the average polarization $\langle P_g \rangle$ induced in the field direction to the field intensity E_0.

The calculation of inclusion responses $\langle \varepsilon_c^g \rangle$ and $\langle \varepsilon_a^g \rangle$ forms the basis for the self-consistent evaluation of the film permittivities ε_c^m and ε_a^m in the effective medium approximation. The unknown values of these permittivities must ensure the equality of the inclusion responses $\langle \varepsilon_c^g \rangle$ and $\langle \varepsilon_a^g \rangle$ to the matric dielectric constants ε_c^m and ε_a^m in the material system under consideration. They can be found by the method of successive approximations using an iterative procedure [19]. In the course of these computations, the values of $\langle \varepsilon_c^g \rangle$ and $\langle \varepsilon_a^g \rangle$ obtained on the previous iteration are assigned to the matrix dielectric constants ε_c^m and ε_a^m used on a current iteration (see Appendix for details).

For the analysis of the Curie-Weiss behavior of ferroelectric thin films, we finally need to specify the temperature dependence of the material parameters involved in Eqs. (13) and (14) and other theoretical

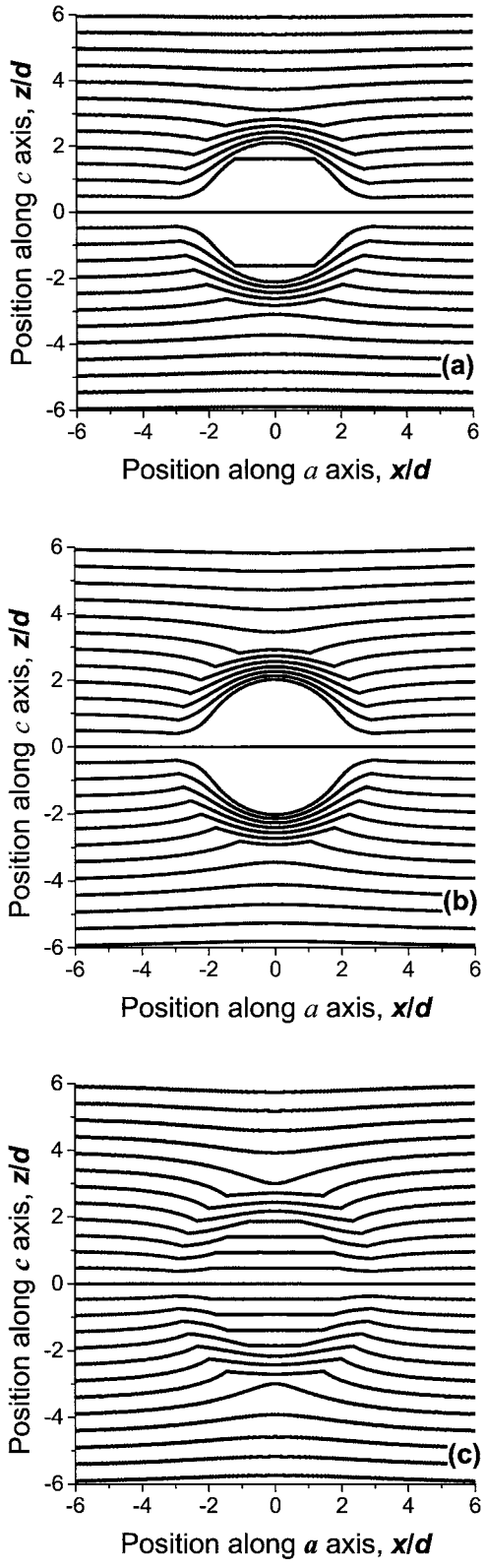

Fig. 4. Maps of equipotential line contours in the coated-inclusion/matrix system subjected to a uniform external electric field $\mathbf{E}_0$. The field $\mathbf{E}_0$ is applied along the symmetry axis c of the material system. The relative permittivities of the inclusion core are taken to be $\varepsilon_c^f = 200$, $\varepsilon_a^f = 20$ (a), $\varepsilon_c^f = 200$, $\varepsilon_a^f = 200$ (b), and $\varepsilon_c^f = 20$, $\varepsilon_a^f = 200$ (c). Dielectric properties of the interface layer and matrix are assumed to be isotropic; their relative permittivities are $\varepsilon_d = 10$ and $\varepsilon_m = 50$, respectively. The radius of inclusion equals 2, and the radius of the outer sphere, where the field was set equal to $\mathbf{E}_0$ during the numerical computations, is taken to be 10 (in units of the interface-layer thickness d). For the isotropic case ($\varepsilon_c^f = \varepsilon_a^f$), the potential Φ was calculated from analytic relations similar to Eqs. (1)–(3). The values of Φ on neighboring equipotential lines differ by $0.5E_0d$. The potential Φ in the center of inclusion is taken to be zero.

relations. Evidently, the dependence of ε_c^m and ε_a^m on temperature mainly results from the variation of the dielectric stiffness $\alpha_1 = (T - \theta)/(2\varepsilon_0 C)$ of the grain cores. Changes of the electrostrictive constants Q_{ij}, elastic compliances s_{ij}, and the grain-boundary permittivity ε_d may be neglected. However, the temperature dependence of the misfit strain S_m in the heterostructure should be taken into account [12]. This strain is defined by the relation $S_m = (b^* - a_0)/a_0$, where $a_0(T)$ is the equivalent unit cell constant of the free-standing film, and $b^*(T)$ is the effective lattice parameter of the substrate. The value of b^* may differ considerably from the actual substrate lattice parameter b because it allows for inelastic strain relaxation in the film/substrate system, e.g., via the generation of misfit dislocations at the interface [20]. Assuming that the strain relaxation becomes suppressed below the growth (annealing) temperature T_g [12], we can calculate the effective lattice parameter b^* from the relation $b^*(T) = b^*(T_g) + b(T) - b(T_g)$. In the first approximation, this leads to a *linear* temperature dependence of the misfit strain S_m, defined by the difference in the mean thermal expansion coefficients of the film and substrate [12]. In this work, however, the strain $S_m(T)$ was calculated with the full account of the nonlinear temperature dependences of lattice parameters a_0 and b given in Refs. [21, 22]. As usual, the film was assumed to be fully relaxed at the growth temperature, i.e. $b^*(T_g) = a_0(T_g)$.

Numerical calculations were performed for polycrystalline BT films grown on representative "tensile" and "compressive" substrates, which induce positive and negative misfit strains $S_m(T)$ in the film, respectively. It was found that the temperature dependences of both the out-of-plane and in-plane film permittivities, ε_c^m and ε_a^m, obey the Curie-Weiss law with a good accuracy. However, the renormalized Curie-Weiss parameters θ_c^* and C_c^*, which determine the dependence $\varepsilon_c^m(T)$, may be substantially different from the parameters θ_a^* and C_a^*, characterizing the variation of $\varepsilon_a^m(T)$.

The dependence of the apparent Curie-Weiss temperatures and constants on the grain size has been analyzed for BT films grown on Si ("tensile" substrate). To allow for the uniform distribution of the spatial orientations of crystal lattices in an ensemble of grains, which is expected to exist in fine-grained films, the electrostrictive constants Q_{ij} involved in Eqs. (13) and (14) were approximated by orientation averages of the single-crystal constants of BT ($Q_{11} = 0.063$ m^4/C^2, $Q_{12} = -0.018$ m^4/C^2, see Ref. [23]) Since the elastic compliances s_{ij} are only weakly sensitive to the lattice orientation in the paraelectric phase, their single-crystal values $s_{11} = 8.3 \times 10^{-12}$ Pa^{-1} and $s_{12} = -2.7 \times 10^{-12}$ Pa^{-1} [17] were used in the calculations. Figure 5 shows the grain-size dependence of the parameters θ_c^* and C_c^* characterizing the out-of-plane permittivity ε_c^m, which was computed for a BT film with the grain-boundary characteristics $d = 0.7$ nm and $\varepsilon_d = 17$ (see below). We see that both the apparent Curie-Weiss temperature and constant decrease monotonically with decreasing grain size. This behavior is qualitatively similar to that demonstrated by a bulk BT ceramic (see Fig. 3),

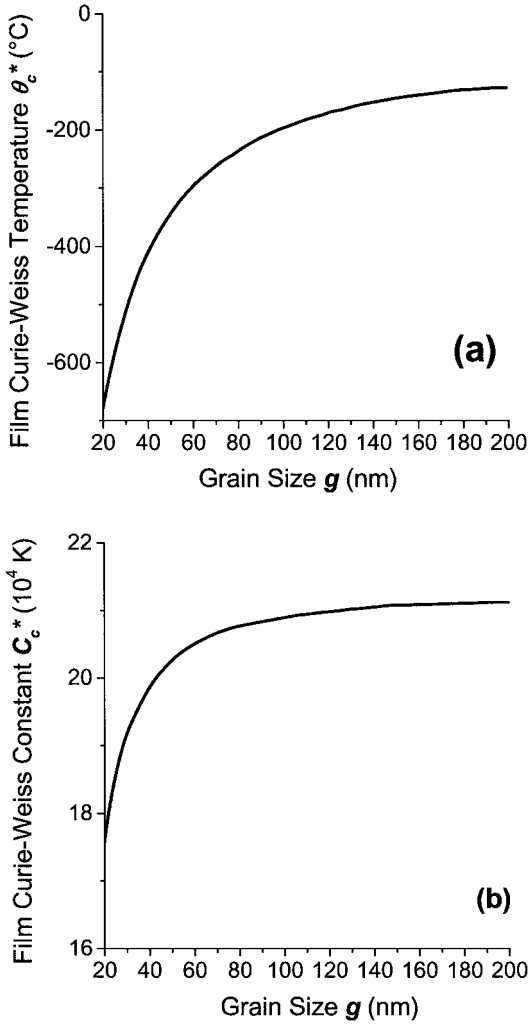

Fig. 5. Apparent Curie-Weiss temperature θ_c^* (a) and constant C_c^* (b) of the film out-of-plane dielectric response ε_c^m as a function of grain size. Theoretical computations were performed for polycrystalline $BaTiO_3$ thin films grown on Si. The grain boundary thickness and permittivity were assumed to be $d = 0.7$ nm and $\varepsilon_d = 17$.

though the absolute values of $\theta_c^*(g)$ and $C_c^*(g)$ may differ markedly from the parameters $\theta^*(g)$ and $C^*(g)$ of a bulk polycrystal.

In conclusion of this section it should be noted that the low-temperature limit, T_c, of the Curie-Weiss behavior in ferroelectric films strongly depends on the substrate material. Indeed, the temperature T_c of the ferroelectric phase transition is a function of the misfit strain S_m in the heterostructure, and $T_c(S_m)$ may be much higher than the Curie temperature of the bulk crystal [18]. If the ferroelectric possesses a finite conductivity like BT, the grain boundaries are expected to have a minor effect on the film transition temperature $T_c(S_m)$ [24]. For a fully textured BT film, the temperature T_c of the (second-order) ferroelectric phase transition may be evaluated using Eqs. (13) and (14) since it corresponds to the divergence of the out-of-plane ε_c^f ("compressive" substrate) or in-plane ε_a^f ("tensile" substrate) permittivity of the grain core [18].

4.2. *Comparison between the Theory and Experiment*

Our theoretical predictions may be compared with the grain-size effect on the dielectric properties, which was observed in polycrystalline BT films grown on platinum coated silicon substrates [11]. These films were prepared by the chemical solution deposition method and had three different microstructures: (1) fine-grained structure with the mean grain size $\langle g \rangle = 30$ nm, (2) grainy microstructure with $\langle g \rangle = 80$ nm, and (3) columnar structure with the mean in-plane grain size $\langle g \rangle = 160$ nm. The temperature dependence of the permittivity ε_c in the film thickness direction was determined at 10 kHz in a plate-capacitor setup. The actual macroscopic dielectric response of a BT film was extracted from the measured capacitance values $c(T)$ via the well-known relation $\varepsilon_c = H/[\varepsilon_0(c^{-1} - c_i^{-1})]$. Here $H \sim 250$ nm is the film thickness, and c_i is the interfacial capacitance, which is due to the presence of "dead" subsurface layers [25] at the film/electrode interfaces. Using the value of $c_i = 0.07$ F/m^2, we obtained the temperature dependences of the actual permittivity of BT films that are shown in Fig. 6. The above value of the interfacial capacitance is appropriate in view of the experimental estimates of $c_i = (0.057 - 0.145)$ F/m^2, which were derived from the thickness dependence of the inverse capacitance of (Ba,Sr)TiO_3 films [26–28].

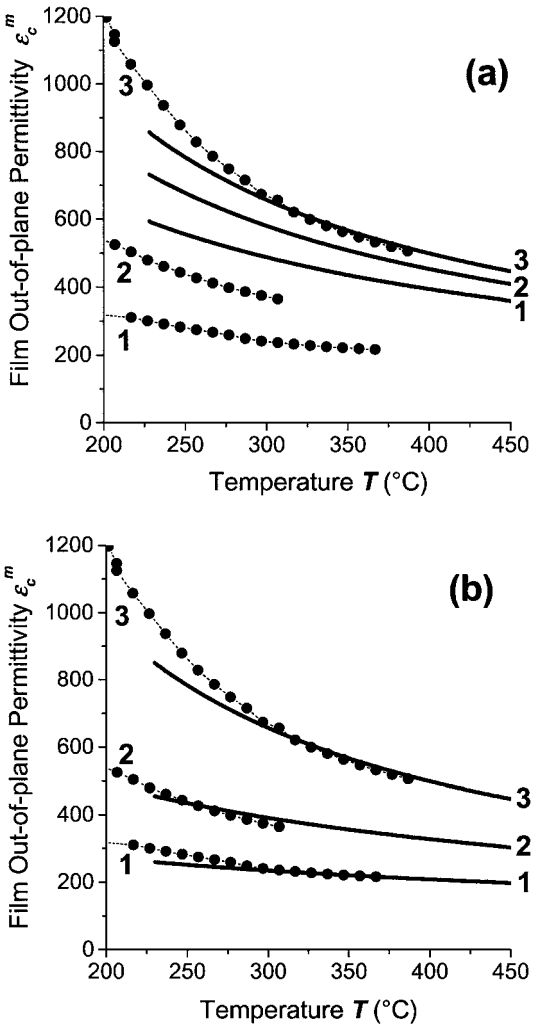

Fig. 6. Temperature dependence of the out-of-plane permittivity ε_c^m of polycrystalline $BaTiO_3$ thin films grown on Si. Circles represent the experimental data corrected for the presence of "dead" layers with the capacitance $c_i = 0.07$ F/m^2 near the film/electrode interfaces. The mean grain size $\langle g \rangle$ in the film equals 30 nm (1), 80 nm (2), and 160 nm (3). The solid curves 1 and 2 show the results of theoretical computations performed in the effective medium approximation at $g = 30$ nm and 80 nm, respectively. The thickness of grain boundaries is taken as $d = 0.7$ nm, and their permittivity is assumed to be $\varepsilon_d = 100$ (a) or $\varepsilon_d = 17$ (b). The theoretical curve 3 is calculated without the account of the grain-boundary effect on ε_c^m.

The analysis of the experimental data shown in Fig. 6 demonstrates that the high-temperature part of $\varepsilon_c(T)$ obeys the Curie-Weiss law with a good accuracy. The values of the apparent Curie-Weiss temperature and constant (for the range of $T > 225$°C) were found to be $\theta_c^* \approx -190$°C, $C_c^* \approx 1.17 \times 10^5$ K ($\langle g \rangle = 30$ nm),

$\theta_c^* \approx -27^\circ$C, $C_c^* \approx 1.2 \times 10^5$ K ($\langle g \rangle = 80$ nm), and $\theta_c^* \approx 42^\circ$C, $C_c^* \approx 1.7 \times 10^5$ K ($\langle g \rangle = 160$ nm). It can be seen that the values of θ_c^* and C_c^* increase gradually with increasing grain size. This behavior is in qualitative agreement with the theoretical predictions (see Fig. 5).

For the quantitative comparison of the theory with the experiment, we performed numerical calculations of the effective out-of-plane permittivity $\varepsilon_c^m(T)$ for three types of polycrystalline BT films, assumed to be grown on Si at $T_g = 800^\circ$C [11]. Two curves $\varepsilon_c^m(T)$ were computed in the effective medium approximation at $g = 30$ nm and 80 nm as described in the previous section. The permittivity and thickness of grain boundaries were taken to be $\varepsilon_d = 100$ and $d = 0.7$ nm based on our results for bulk BT ceramics. The third curve was calculated directly from Eq. (13) to model a columnar-structured film with a large grain size $\langle g \rangle = 160$ nm. Here it was taken into account that the grain-boundary effect on the permittivity of columnar-structured films may be neglected when the in-plane grain size is much larger than the thickness d of these boundaries. At this point we would like to emphasize that the model of a spherical inclusion embedded into an infinite homogeneous matrix (Fig. 1) is valid only for films having a *grainy* microstructure with *equiaxial* crystallites. The grain size must be much smaller than the film thickness to ensure the applicability of the effective medium approximation.

The calculated curves $\varepsilon_c^m(T)$ are presented on Fig. 6(a) together with the experimental data. For the columnar-structured film, the high-temperature behavior of the dielectric response can be reproduced with a reasonable accuracy by choosing the aforementioned value of the interfacial capacitance c_i. In contrast, the observed permittivities of films with the fine-grained and grainy microstructures are much smaller than the theoretically predicted values. This discrepancy can be removed by assuming a lower value of the grain boundary permittivity. As shown in Fig. 6(b), with $\varepsilon_d = 17$ and $d = 0.7$ nm, the calculations give the correct magnitude of the high-temperature dielectric response for both fine-grained and grainy films. The theoretical Curie-Weiss parameters θ_c^* and C_c^*, however, still differ considerably from the measured ones, as can be seen from the slope of the dependences $\varepsilon_c^m(T)$ shown in Fig. 6(b).

Thus, the theoretical analysis of the experimental data indicates that the mean permittivity of grain boundaries in polycrystalline BT films is much lower than in dense BT ceramics. This suppression of the average dielectric response in the grain-boundary regions may be attributed to the porosity of BT films prepared by the chemical solution deposition method. The enhancement of the negative grain-boundary effect due to a larger thickness d of disordered regions between crystallites in thin films also cannot be ruled out. Finally, the fact that the theoretical values of the Curie-Weiss temperature $\theta_c^*(g)$ and constant $C_c^*(g)$ are lower and higher than the experimental estimates, respectively, may be explained by an additional relaxation of the misfit strain during the cooling. This relaxation is equivalent to an effective reduction of the difference between thermal expansion coefficients of the film and substrate and so leads to an increase of θ_c^* and a decrease of C_c^* in BT films grown on tensile substrates [12]. The strain release in polycrystalline films well below the growth temperature $T_g = 800^\circ$C may be caused by mutual shifts of crystallites along the grain boundaries.

5. Conclusions

1. The effect of grain boundaries on the macroscopic dielectric response of bulk ceramics and polycrystalline thin films in the paraelectric regime consists mainly in the renormalization of the Curie-Weiss law. Deviations from the Curie-Weiss behavior, which may be visible in a wide temperature range, become more pronounced in bulk ceramics with the increase of the volume fraction and permittivity of the grain-boundary phase.
2. For bulk ferroelectric ceramics, the apparent Curie-Weiss temperature θ^* decreases monotonically with increasing thickness d and decreasing permittivity ε_d of the grain boundaries, depending mainly on the ratio d/ε_d. The Curie-Weiss constant C^* is independent of the grain-boundary permittivity ε_d but decreases gradually with increasing volume fraction of the grain-boundary phase.
3. In polycrystalline ferroelectric films, the grain boundaries suppress both the out-of-plane and in-plane dielectric responses in the paraelectric regime. The Curie-Weiss parameters of these responses ε_c^m and ε_a^m may be very different from each other due to the mechanical film/substrate interaction. In thin films with a grainy microstructure, the apparent Curie-Weiss temperature θ_c^* decreases monotonically with decreasing grain size g.

Appendix

Since the available finite-element program packages do not enable us to calculate the film permittivities in the effective medium approximation automatically, we have developed our own computation procedure based on the finite-difference method. To that end, the inhomogeneous material system under consideration was divided geometrically into cells by a regular mesh with a variable cell size. In accordance with the symmetry of the coated inclusion, a spherical coordinate system (r, ϕ, θ) was employed in the computations. The material system was first divided into slabs by spherical surfaces with radii $r_i (i = 1, 2, 3, \ldots, n)$. Inside the coating "dead" layer and close to its surfaces the increments $\Delta r_i = r_i - r_{i-1}$ were chosen to be much smaller than outside this region of strong field inhomogeneity. (This is necessary to guarantee a computationally efficient and precise calculation of the electric field distribution.) The spherical slabs were then divided into cells by a set of surfaces corresponding to fixed values of the angles ϕ and θ everywhere.

Inside the inclusion, dead layer, and matrix, the electric potential $\mathbf{\Phi}(\mathbf{r})$ must satisfy Poisson's equation [14]. This differential equation, written in a spherical coordinate system, was transformed into a finite-difference equation [29]. As a result, a system of linear equations was obtained for the unknown values of the potential $\mathbf{\Phi}$ at the nodes of the mesh. The solution of this linear system was obtained by means of the superrelaxation iterative method [29]. The symmetrization of the system matrix was done in the course of calculations, which ensures the convergence of the iterative procedure to the rigorous solution of a system of linear equations [30]. At the center of the inclusion ($r = 0$), the potential $\mathbf{\Phi}$ was taken to be zero, whereas on the outer boundary ($r = r_n$) of the mesh the electric field $\mathbf{E}$ was set equal to a given external field $\mathbf{E}_0$. The latter was assumed to be parallel or perpendicular to the symmetry axis c of the anisotropic inclusion/matrix system in the two basic situations, which were treated separately.

The numerical computations were performed in the following way. Starting from the inclusion center, the potential $\mathbf{\Phi}$ was computed at all nodes from the introduced system of linear equations with the aid of the superrelaxation iterative method. At the nodes, which lay directly on the boundaries between dissimilar dielectric media, the potential $\mathbf{\Phi}$ was quantified using the finite-difference approximation of the continuity condition for the displacement $\mathbf{D}$ [14] (the continuity of tangential components of the electric field $\mathbf{E}$ is provided automatically here). The iterative process in this "forward" direction was carried out until reaching the outer boundary of the mesh ($r = r_n$). Then it was repeated in the "backward" direction, i.e., from the outer boundary to the inclusion center, in order to improve the convergence. By cycling such iterative process back and forth, it is possible to find the solution of the aforementioned system of linear equations to any desired degree of precision. Reducing sizes of the mesh cells on the next stage of computations, we obtained a linear system with larger number of equations, which evidently approximates Poisson's differential equation and the boundary conditions with higher accuracy. The reduction of cell sizes was continued until differences between newly computed values of the potential $\mathbf{\Phi}(\mathbf{r})$ and its preceding values become negligible at all coinciding nodes of two meshes. The final numerical solution for the potential $\mathbf{\Phi}(\mathbf{r})$ then enabled us to determine spatial distribution of the electric field $\mathbf{E}$, displacement $\mathbf{D}$, and the polarization $\mathbf{P}$ inside the inclusion and dead layer. Hence, the average dielectric responses $\langle \varepsilon_c^g \rangle$ and $\langle \varepsilon_a^g \rangle$ of the coated inclusion to the applied fields $\mathbf{E}_0$ parallel and perpendicular to the symmetry axis c were calculated. (It was found that these responses become practically independent of the position r_n of the outer boundary when r_n is about 10 times larger than the inclusion radius.)

The procedure described above was used to carry out self-consistent computations of the permittivities ε_c^m and ε_a^m of polycrystalline BT films. On the first iteration, the matrix dielectric constants ε_c^m and ε_a^m were approximated by simple averages of the permittivities ε_c^f and ε_a^f of the inclusion and the permittivity ε_d of the dead layer. For the resulting inclusion/matrix system, the relevant electrostatic problem was solved in the case of an external field $\mathbf{E}_0$ applied along the symmetry axis c, and the dielectric response $\langle \varepsilon_c^g \rangle$ of the coated inclusion was calculated. Then the computed value of $\langle \varepsilon_c^g \rangle$ was assigned to the matrix permittivity ε_c^m, and the dielectric behavior of this modified inclusion/matrix system was studied under a field $\mathbf{E}_0$ perpendicular to the symmetry axis in order to find the inclusion response $\langle \varepsilon_a^g \rangle$. On the second iteration, the above two-step procedure was repeated with the current values of $\langle \varepsilon_c^g \rangle$ and $\langle \varepsilon_a^g \rangle$ assigned to the matrix dielectric constants ε_c^m and ε_a^m. The inclusion responses $\langle \varepsilon_c^g \rangle$ and $\langle \varepsilon_a^g \rangle$ were updated, and their refined values were used to define the matrix permittivities ε_c^m and ε_a^m on the third iteration. This iterative process was continued until the difference

between two successive approximations for the inclusion responses $\langle \varepsilon_c^g \rangle$ and $\langle \varepsilon_a^g \rangle$ becomes negligible. Thus obtained final values of $\langle \varepsilon_c^g \rangle$ and $\langle \varepsilon_a^g \rangle$ were regarded as the out-of-plane (ε_c^m) and in-plane (ε_a^m) effective permittivities of a polycrystalline film.

Acknowledgment

The research described in this publication was made possible in part by Grant No. I/75965 from the Volkswagen-Stiftung, Germany.

Note

1. Equations (1)–(3) also describe the cases where a conductor (relative permittivity $\varepsilon = \infty$) or vacuum gap ($\varepsilon = 1$) is present in the material system. In particular, a thin conducting interface layer ($\varepsilon_d = \infty$) leads to a full screening of the dielectric inclusion ($\mathbf{E}^{(f)} = 0$). Besides, in the limiting case of $d = 0$ (interface layer is absent), Eqs. (1)–(3) reduce to a well-known expression for the field inside and outside a dielectric sphere surrounded by a dissimilar matrix which is subjected to a uniform electric field (Ref. [14]).

References

1. N. Setter and R. Waser, *Acta Mater.*, **48**, 151 (2000).
2. M.H. Frey and D.A. Payne, *Phys. Rev. B*, **54**, 3158 (1996).
3. M.P. McNeal, S.-J. Jang, and R.E. Newnham, *J. Appl. Phys.*, **83**, 3288 (1998).
4. H. Kniepkamp and W. Heywang, *Z. Angew. Phys.*, **9**, 385 (1954).
5. K. Kinoshita and A. Yamaji, *J. Appl. Phys.*, **47**, 371 (1976).
6. G. Arlt, D. Hennings, and G. de With, *J. Appl. Phys.*, **58**, 1619 (1985).
7. W.R. Buessem, L.E. Cross, and A.K. Goswami, *J. Am. Ceram. Soc.*, **49**, 33 (1966).
8. M.N. Frey, Ph.D. Thesis, University of Illinois at Urbana-Champaign, 1996.
9. M.H. Frey, Z. Hu, P. Han, and D.A. Payne, *Ferroelectrics*, **206/207**, 337 (1998).
10. D.A. Payne and L.E. Cross, in *Microstructure and Properties of Ceramic Materials*, edited by T.S. Yen and J.A. Pask (Science Press, Beijing, 1984).
11. S. Hoffmann and R. Waser, *J. Phys. IV*, **8**, 9 (1998).
12. N.A. Pertsev, A.G. Zembilgotov, S. Hoffmann, R. Waser, and A.K. Tagantsev, *J. Appl. Phys.*, **85**, 1698 (1999).
13. M. Marutake, *J. Phys. Soc. Jpn.*, **11**, 807 (1956).
14. L.D. Landau, E.M. Lifshits, and L.P. Pitaevskii, *Electrodynamics of Continuous Media* (Pergamon, Oxford, 1984).
15. L.D. Landau and E.M. Lifshits, *The Classical Theory of Fields* (Pergamon, Oxford, 1971).
16. A.J. Moulson and J.M. Herbert, *Electroceramics: Materials, Properties, Applications* (Chapman and Hall, London, 1990).
17. F. Jona and G. Shirane, *Ferroelectric Crystals* (Macmillan, New York, 1962).
18. N.A. Pertsev, A.G. Zembilgotov, and A.K. Tagantsev, *Phys. Rev. Lett.*, **80**, 1988 (1998).
19. N.A. Pertsev, A.G. Zembilgotov, and R. Waser, *J. Appl. Phys.*, **84**, 1524 (1998); *Phys. Solid State*, **40**, 2002 (1998).
20. J.S. Speck and W. Pompe, *J. Appl. Phys.*, **76**, 466 (1994).
21. Y.S. Touloukian, R.K. Kirby, R.E. Taylor, and T.Y.R. Lee, *Thermal Expansion, Nonmetallic Solids*, Thermophysical Properties of Matter, Vol. 13 (Plenum, New York, 1997).
22. Landolt-Börnstein, *Numerical Data and Functional Relationships in Science and Technology*, New Series, Vol. III/29a (Springer, Berlin, 1992).
23. A.F. Devonshire, *Phil. Mag.*, **42**, 1065 (1951).
24. H. Kohlstedt, N.A. Pertsev, and R. Waser, *Mat. Res. Soc. Symp. Proc.*, **688**, C6.5.1 (2002).
25. C. Zhou and D.M. Newns, *J. Appl. Phys.*, **82**, 3081 (1997).
26. S. Zafar, R.E. Jones, P. Chu, B. White, B. Jiang, D. Taylor, P. Zurcher, and S. Gillepsie, *Appl. Phys. Lett.*, **72**, 2820 (1998).
27. S.K. Streiffer, C. Basceri, C.B. Parker, S.E. Lash, and A.I. Kingon, *J. Appl. Phys.*, **86**, 4565 (1999).
28. M.C. Werner, I. Banerjee, P.C. McIntyre, N. Tani, and M. Tanimura, *Appl. Phys. Lett.*, **77**, 1209 (2000).
29. G.A. Korn and T.M. Korn, *Mathematical Handbook for Scientists and Engineers* (McGraw-Hill, New York, 1968).
30. D.K. Faddeev and V.N. Faddeeva, *Numerical Methods of Linear Algebra* (State Publish. House of Phys.-Math. Literature, Moscow-Leningrad, 1963, in Russian).